NANO LETTERS

Letter

pubs.acs.org/NanoLett

Observation of Intervalley Biexcitonic Optical Stark Effect in Monolayer WS_2

Edbert J. Sie,[†] Chun Hung Lui,[‡] Yi-Hsien Lee,[§] Jing Kong,[∥] and Nuh Gedik*[,†]

[†]Department of Physics, Massachusetts Institute of Technology, Cambridge, Massachusetts 02139, United States

[‡]Department of Physics and Astronomy, University of California, Riverside, California 92521, United States

[§]Materials Science and Engineering, National Tsing-Hua University, Hsinchu 30013, Taiwan

[∥]Department of Electrical Engineering and Computer Science, Massachusetts Institute of Technology, Cambridge, Massachusetts 02139, United States

Supporting Information

ABSTRACT: Coherent optical driving can effectively modify the properties of electronic valleys in transition metal dichalcogenides. Here, we observe a new type of optical Stark effect in monolayer WS_2, one that is mediated by intervalley biexcitons under the blue-detuned driving with circularly polarized light. We find that such helical optical driving not only induces an exciton energy downshift at the excitation valley but also causes an anomalous energy upshift at the opposite valley, which is normally forbidden by the exciton selection rules but now made accessible through the intervalley biexcitons. These findings reveal the critical, but hitherto neglected, role of biexcitons to couple the two seemingly independent valleys, and to enhance the optical control in valleytronics.

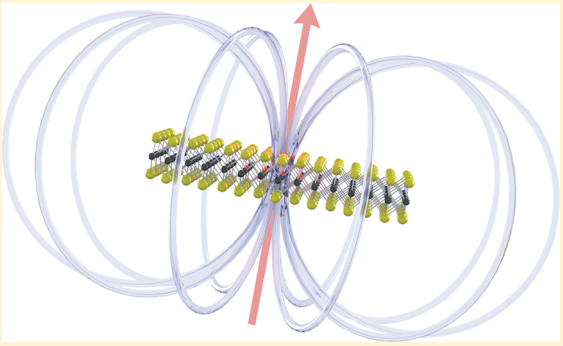

KEYWORDS: *WS_2, valley, biexciton, blue detuned, optical Stark effect, ultrafast optics*

Monolayer transition metal dichalcogenides (TMDs) host tightly bound excitons in two degenerate but inequivalent valleys (K and K′), which can be selectively photoexcited using left (σ^-) or right (σ^+) circularly polarized light (Figure 1a).[1−4] The exciton energy levels can be tuned optically in a valley-selective manner by means of the optical Stark effect.[5,6] Prior research has demonstrated that monolayer TMDs driven by below-resonance (red-detuned) circularly polarized light can exhibit an upshifted exciton level, either at the K or K′ valleys depending on the helicity, while keeping the opposite valley unchanged. This valley-specific phenomenon arises from the exciton state repulsion by the photon-dressed (Floquet) state in the same valley, a mechanism consistent with the optical Stark effect in other solids.[7,8]

Despite much recent progress, a complete understanding of the optical Stark effect in monolayer TMDs is still lacking. First, the downshift of exciton level, an anticipated complementary effect using above-resonance (blue-detuned) optical driving, has not been demonstrated. This is challenging because the blue-detuned light excites real exciton population, which can easily obscure the optical Stark effect. Second, when the detuning is sufficiently small and comparable to the biexciton binding energy, the effect may involve a coherent formation of the recently identified intervalley biexcitons.[9,10] These biexcitons are expected to contribute to the optical Stark effect, as indicated by earlier studies in semiconductor quantum wells.[11,12] Elucidating these processes is therefore crucial to understand the coherent light-matter interactions in monolayer TMDs.

In this Letter, we explore the optical Stark effect in monolayer WS_2 under blue-detuned optical driving. By pumping the system above the A exciton resonance using left-circularly polarized laser pulses, we can lower the exciton energy at the K valley. In addition, as the driving photon energy approaches the resonance, an unexpected phenomenon emerges: the exciton energy at the opposite (K′) valley is raised. This observation is anomalous because interaction with the driving photon is forbidden at this valley by the exciton selection rules. The upshifted exciton level also contrasts sharply with the downshifted level at the K valley. These findings reveal the strong influence of intervalley biexcitons on the optical Stark effect. By including their contributions in an expanded four-level scheme of optical Stark effect, we are able to account for all the main observations in our experiment.

We monitor the pump-induced change of exciton levels at the K (K′) valley by using the reflection of synchronized broadband probe pulses with σ^- (σ^+) polarization (Figure 1b, see also Supporting Information). Our samples are high-quality WS_2 monolayers grown by chemical vapor deposition on sapphire substrates.[13−15] The change of absorption ($\Delta\alpha$) in

Received: July 19, 2016
Revised: November 21, 2016
Published: November 30, 2016

ACS Publications © 2016 American Chemical Society

DOI: 10.1021/acs.nanolett.6b02998
Nano Lett. 2016, 16, 7421−7426

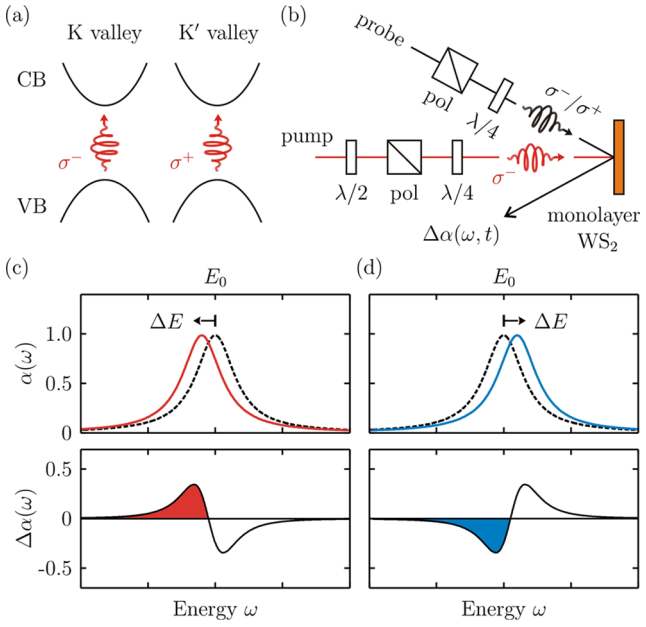

Figure 1. (a) K and K′ valleys couple selectively with left (σ^-) and right (σ^+) circularly polarized light due to selection rules. (b) Schematic of the pump−probe spectroscopy setup. (c,d) Simulated absorption spectra $\alpha(\omega)$ that are shifted by ΔE to lower and higher energies (upper panels), as well as their induced absorption spectra $\Delta\alpha(\omega)$ (lower panels).

monolayer WS_2 can be extracted from the change of reflection by using Kramers−Kronig analysis within a thin-film approximation.[10,16] The resulting $\Delta\alpha$ spectrum typically shows a single-cycle waveform, which allows us to determine the direction and magnitude of the exciton energy shift (ΔE) (Figure 1c,d). In our experiment, we examine the lower-energy part of $\Delta\alpha$ spectrum (filled color in Figure 1c,d) because the coherent contribution is more pronounced below the energy resonance (E_0). For a blue-detuned optical Stark effect (Figure 2a), the pump photon energy lies slightly higher than the A exciton resonance in monolayer WS_2, which is at E_0 = 2.00 eV from our measured absorption spectrum (Figure 2b) as well as from other experiments.[16] We observe no side peak or shoulder below the exciton absorption peak, implying that our samples have weak trionic effect (Figure 2b).

Figure 2c shows the $\Delta\alpha$ spectra at zero pump−probe delay at three different pump photon energies ($h\nu$ = 2.10, 2.07, 1.99 eV) but the same pump fluence (28 μJ/cm^2). We display the spectra in the range of 1.80−1.96 eV, where the coherent effect is more pronounced and less contaminated by the pump scattering. For the σ^- probe (Figure 2c), the spectral shape is similar to that in Figure 1c, indicating a redshift of the exciton level at the same (K) valley. As the pump photon energy approaches the resonance from 2.10 to 1.99 eV, the magnitude increases considerably, indicating an increasing redshift of the exciton level. This observation complements the previous studies, which reported a blueshift under red-detuned optical

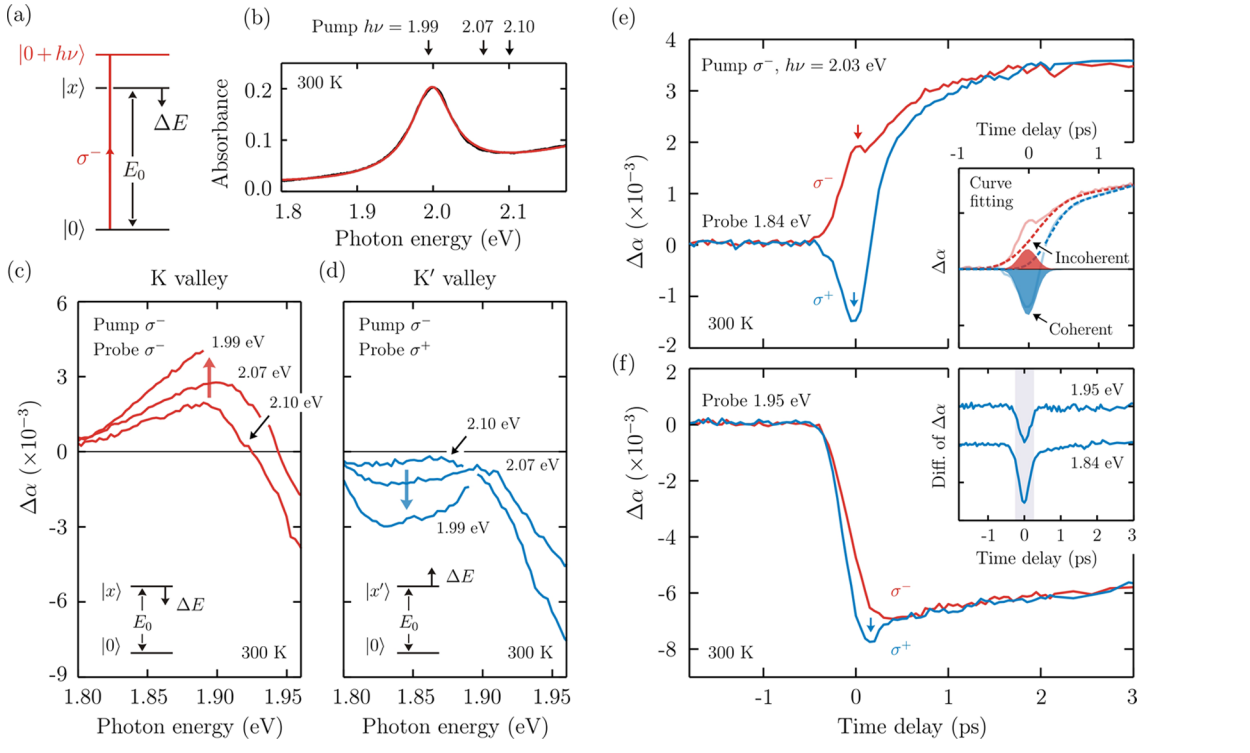

Figure 2. Blue-detuned optical Stark effect and its observation in monolayer WS_2. (a) Blue-detuned optical driving scheme, where we use σ^- pump pulse with photon energy $h\nu$ slightly above the exciton resonance E_0. (b) Measured absorption spectrum of monolayer WS_2 shows that E_0 = 2.00 eV at 300 K (black curve), which can be fitted with a single Lorentzian (neutral) exciton peak plus a background polynomial slope from the higher energy states (red curve). (c,d) Valley-specific $\Delta\alpha$ spectra induced by σ^- pump pulses ($h\nu$ = 1.99, 2.07, 2.10 eV) and monitored by using σ^-(K) and σ^+(K′) broadband probe pulses at pump−probe time delay Δt = 0. The increasing $\Delta\alpha$ at K valley indicates a pump-induced redshift of exciton energy. On the other hand, the decreasing $\Delta\alpha$ at K′ valley, though unexpected, indicates a pump-induced blueshift of exciton energy. (e,f) Time traces of $\Delta\alpha$ induced by σ^- pump pulses ($h\nu$ = 2.03 eV) and monitored at probe energy of 1.84 and 1.95 eV with different helicities. The top inset shows the curve fitting decomposition of the coherent and incoherent signals. The bottom inset shows the valley contrast of the signals, $\Delta\alpha(\sigma^+) - \Delta\alpha(\sigma^-)$, where the two curves are offset for clarity.

DOI: 10.1021/acs.nanolett.6b02998
Nano Lett. 2016, 16, 7421−7426

driving. In contrast, the $\Delta\alpha$ spectra at the opposite (K′) valley exhibit a distinct form, as revealed by the σ^+ probe (Figure 2d). Its value is negative in the range of 1.80−1.90 eV with a waveform similar to that in Figure 1d. This indicates a blueshift of the exciton level at the K′ valley, which becomes more substantial as the pump approaches the resonance (see Supporting Information for more discussions on both blue- and red-detuned pumping).

The observed spectra include both the coherent signals from the optical Stark effect and the incoherent signals from the exciton population that is unavoidably generated by the above-resonance optical pumping.[9,10,17−24] The coherent signals are known to appear only within the pump pulse duration, whereas the incoherent signals remain after the pulsed excitation. Their different time dependences allow us to separate them by monitoring the temporal evolution of $\Delta\alpha$. Figure 2e,f shows the time traces after the excitation with 200 fs laser pulses at photon energy $h\nu$ = 2.03 eV. At pump−probe delay Δt > 1 ps, $\Delta\alpha$ is similar for both valleys with positive value at the probe energy of 1.84 eV but negative value at 1.95 eV. These features correspond to the exciton population effects, where the slow rise in Figure 2e shares the same time scale with the intervalley scattering. This suggests that the initial population-induced dynamics arises from the same scattering mechanism, which can be mediated by defects and electron−phonon interactions. At zero pump−probe delay, however, the two valleys exhibit significantly different response. The difference can be attributed to the optical Stark effect, a coherent process that follows the pump pulse intensity profile. At probe energy 1.84 eV, the coherent contribution is particularly prominent and can be readily separated from the incoherent background by direct extrapolation (insets of Figure 2e,f and Figure S3 in the Supporting Information).

We have extracted the coherent component of $-\Delta\alpha$ at 1.84 eV and plot the values as a function of pump fluence (Figure 3).

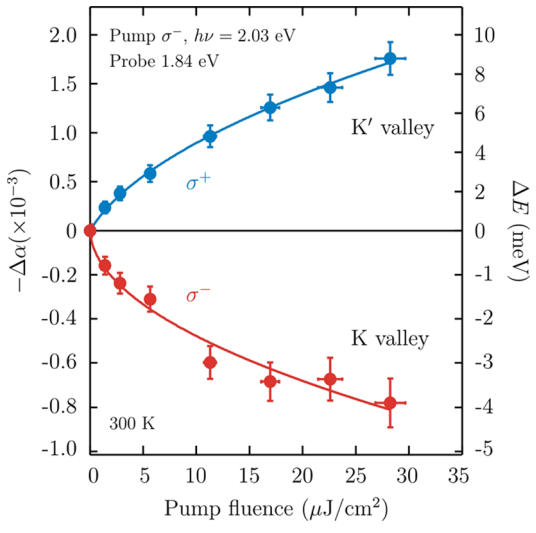

Figure 3. Fluence dependence of the blue-detuned optical Stark shift. The measured data of $-\Delta\alpha$ ($\propto\Delta E$) are plotted at increasing pump fluence (σ^-, $h\nu$ = 2.03 eV), measured valley-selectively at probe energy of 1.84 eV. The energy scale on the right axis is estimated based on the measured absorption slope of 0.2/eV at 1.84 eV. Note that the energy scaling is different between the two valleys. The fitting curves show that the K and K′ valleys exhibit square-root fluence dependences, as discussed in the main text.

The associated energy shift ΔE can be estimated from the differential form $\Delta\alpha(\omega, \Delta E) = -(d\alpha/d\omega)\Delta E$.[25] Given the measured $-\Delta\alpha$ and the slope at 1.84 eV, we have evaluated such energy shift (the right vertical axis of Figure 3). Our result shows that the exciton level at K and K′ valleys respectively downshifts (−4 meV) and upshifts (+9 meV) under the σ^- blue-detuned optical driving. The magnitude of both shifts increases sublinearly with pump fluence, which is in contrast to the linear fluence dependence in prior red-detuned experiments.

We can exclude other incoherent processes as the responsible mechanism for the observed valley-contrastive energy shifts at time-zero. The population-induced biexciton absorption, Pauli blocking and renormalization of band structure should not be responsible, because they normally persist as long as the exciton recombination time (>1 ps). The exciton population imbalance between the K and K′ valleys lasts for ∼1 ps, still longer than the pulse duration of our pump laser (∼200 fs). But it may contribute to the slow rise (∼1 ps) of valley-contrastive signal in Figure 2e, possibly due to a small renormalization of band structure. In respect to a possible exciton−exciton interaction, excitons in the same (different) valley are expected to repel (attract) one another and cause a blue (red) shift of the exciton energy in analogy to the spin-dependent interactions of excitons in semiconductor quantum wells.[26,27] These predicted valley-dependent energy shifts are, however, opposite to the energy shifts in our experiment. We can therefore conclude that the valley-contrastive energy shift is a coherent phenomenon.

The upshift of exciton level at the K′ valley is anomalous. First, according to the well-known selection rules in monolayer WS_2, the K′ valley is not accessible by the σ^- (K valley) optical driving. The observed optical Stark effect at K′ valley apparently violates this selection rule. Second, even if the access to the K′ valley is allowed, a blue-detuned optical driving is expected to downshift the exciton level, as in the case of the K valley. The energy upshift at the K′ valley apparently defies this common knowledge of optical Stark effect, hence it must arise from a different mechanism, one that is beyond the framework of interaction between light and single excitons.

We attribute this phenomenon to the optical Stark effect that is mediated by intervalley biexcitons. Recent research has revealed significant interactions between individual excitons in monolayer TMDs. In particular, two excitons at different valleys can be bound to form an excitonic molecule, the intervalley biexciton, with unusually large binding energies (Δ_b = 40−70 meV).[9,10,28−30] These intervalley biexcitons offer an effective channel to couple the two valleys with selection rules different from those of single excitons. In view of such strong biexcitonic effect, we can account for our observations within a four-level scheme (Figure 4), which includes the ground state $|0\rangle$, the two valley exciton states $|x\rangle$ and $|x'\rangle$, and the intervalley biexciton state $|xx'\rangle$. In this scheme, the optical pumping creates two types of photon-dressed (Floquet) states, one from the ground state $|0 + h\nu\rangle$ and the other from the biexciton state $|xx' - h\nu\rangle$. The former can interact with the exciton state $|x\rangle$ at the K valley. Because $|0 + h\nu\rangle$ lies above $|x\rangle$ in a blue-detuned experiment, repulsion between the two states causes $|x\rangle$ to downshift. This is responsible for the ordinary optical Stark effect at the K valley (red dots in Figure 3). In contrast, the biexciton Floquet state $|xx' - h\nu\rangle$ can interact with the exciton state $|x'\rangle$ at the opposite (K′) valley according to different selection rules for the intervalley biexciton. Because $|xx' - h\nu\rangle$ lies below $|x'\rangle$, repulsion between the two will cause $|x'\rangle$ to

DOI: 10.1021/acs.nanolett.6b02998
Nano Lett. 2016, 16, 7421−7426

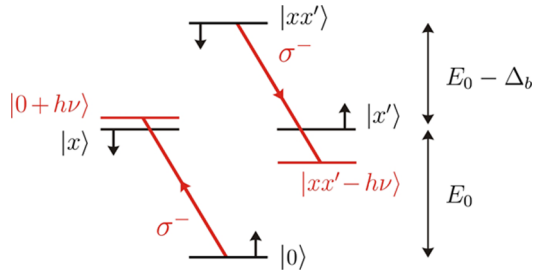

Figure 4. Energy level diagram of the intervalley biexcitonic optical Stark effect. Here the σ^- pump pulse is blue-detuned above the energy resonance between the ground state $|0\rangle$ and the exciton state $|x\rangle$. Coherent absorption from $|0\rangle$ results in a photon-dressed state $|0 + h\nu\rangle$, while coherent emission from the intervalley biexciton state $|xx'\rangle$ results in a photon-dressed state $|xx' - h\nu\rangle$. Additional states $|x - h\nu\rangle$ and $|x' + h\nu\rangle$ also arise in this situation, but we omit them from this figure for the sake of clarity. These additional states are included in Supporting Figure S4.

upshift. This is responsible for the anomalous optical Stark effect at the K′ valley (blue dots in Figure 3). It is evident that the intervalley biexciton plays a unique role in coupling the two valleys, and the effect can be utilized for enhanced control of valley degree of freedom.[31]

In order to investigate the photoinduced coupling between these states, we consider a four-level Jaynes-Cummings model with a procedure similar to but extended from our previous work[5,32] (see details in the Supporting Information). Such a model has been successfully applied to describe the light-dressed states in many semiconductor systems and can readily be adopted to describe the exciton−biexciton system.[5,7,8,33−35] By virtue of the unique valley selection rules in this system, the originally 4 × 4 Hamiltonian matrix can be simplified into two decoupled 2 × 2 Hamiltonian matrices

$$\begin{aligned}\hat{H}_{\mathrm{K}} &= \tfrac{1}{2}E_0\hat{\sigma}_z + h\nu\hat{a}^+\hat{a} + \tfrac{1}{2}g(\hat{\sigma}^+\hat{a} + \hat{\sigma}^-\hat{a}^+)\\ \hat{H}_{\mathrm{K}'} &= \tfrac{1}{2}(E_0 - \Delta_b)\hat{\sigma}_z + h\nu\hat{a}^+\hat{a} + \tfrac{1}{2}g'(\hat{\sigma}^+\hat{a} + \hat{\sigma}^-\hat{a}^+)\end{aligned} \tag{1}$$

The three terms from left to right in each Hamiltonian correspond to the two-level system, the photon reservoir, and the exciton-photon interactions, respectively. Possible contribution from real exciton population is neglected in this model. Here, g and g' are the exciton−photon coupling strengths, $\hat{\sigma}$(s) are the Pauli matrices, $\hat{a}$ and $\hat{a}^+$ are the photon ladder operators, and Δ_b is the biexciton binding energy. The Hamiltonian $\hat{H}_{\mathrm{K}}$ couples states $|0, n+1\rangle$ and $|x, n\rangle$, while $\hat{H}_{\mathrm{K}'}$ couples states $|x', n\rangle$ and $|xx', n-1\rangle$, where n is the number of photons. By using these states as the basis, we can express the Hamiltonians as the following matrices

$$\begin{aligned}H_{\mathrm{K}} &= \frac{1}{2}\begin{pmatrix} h\nu - E_0 & g\sqrt{n+1} \\ g\sqrt{n+1} & -(h\nu - E_0)\end{pmatrix}\\ H_{\mathrm{K}'} &= \frac{1}{2}\begin{pmatrix} h\nu - E_0 + \Delta_b & g'\sqrt{n} \\ g'\sqrt{n} & -(h\nu - E_0 + \Delta_b)\end{pmatrix}\end{aligned} \tag{2}$$

Here we omit the energy offset $h\nu(n \pm 1/2)$ of the photon reservoir. Diagonalization of the Hamiltonian matrices gives the eigenenergies of the photon-dressed states $E_{\mathrm{K}} = \pm\frac{1}{2}\sqrt{(h\nu - E_0)^2 + g^2(n+1)}$ and $E_{\mathrm{K}'} = \pm\frac{1}{2}\sqrt{(h\nu - E_0 + \Delta_b)^2 + g'^2(n)}$, where $g\sqrt{n+1} = \mathcal{M}\mathcal{E}_0$ and $g'\sqrt{n} = \mathcal{M}'\mathcal{E}_0$ are the Rabi frequencies. Here $\mathcal{M}$ and $\mathcal{M}'$ are the moments for $|0\rangle \rightarrow |x\rangle$ and $|x'\rangle \rightarrow |xx'\rangle$ transitions, respectively, and $\mathcal{E}_0$ is the electric field amplitude of the light. From these expressions, we can finally obtain the optical Stark shifts of the exciton levels

$$\begin{aligned}\Delta E_{\mathrm{K}} &= -\frac{1}{2}\left(\sqrt{(h\nu - E_0)^2 + \mathcal{M}^2\mathcal{E}_0^2} - (h\nu - E_0)\right)\\ \Delta E_{\mathrm{K}'} &= \frac{1}{2}\left(\sqrt{(h\nu - E_0 + \Delta_b)^2 + \mathcal{M}'^2\mathcal{E}_0^2}\right.\\ &\quad \left. - (h\nu - E_0 + \Delta_b)\right)\end{aligned} \tag{3}$$

Despite much similarity, the two optical Stark effects are quantitatively different, because the transition moments are generally different and the biexciton Floquet state is offset by Δ_b. In the large detuning limit $h\nu - E_0 \gg \mathcal{M}\mathcal{E}_0$, we retrieve the well-known expression $\Delta E_{\mathrm{K}} = -\mathcal{M}^2\mathcal{E}_0^2/4(h\nu - E_0)$ with a linear fluence dependence, as observed in the previous red-detuned experiment. Conversely, in the small detuning limit $h\nu - E_0 \ll \mathcal{M}\mathcal{E}_0$, we obtain $\Delta E_{\mathrm{K}} = -\frac{1}{2}\sqrt{\mathcal{M}^2\mathcal{E}_0^2}$ with a square-root fluence dependence. The observed sublinear fluence dependence in Figure 3 indicates that the small-detuning limit is reached for both valleys in our experiment. Our fluence dependence data can be fitted with this model (Figure 3) with transition moments and effective detunings as adjustable parameters (Supporting Information). The good agreement between the experiment and the model strongly supports that this optical Stark effect is mediated by intervalley biexcitons. We note that trion states can in principle also exhibit an optical Stark effect. However, given the small charge background with no trion absorption feature in our samples (Figure 2b), we do not expect the trion states to play a significant role in our observation.

In summary, we have observed an exciton energy downshift at the excitation (K) valley and an energy upshift at the opposite (K′) valley under the blue-detuned optical driving in monolayer WS_2. While the energy downshift arises from the single-exciton optical Stark effect, the anomalous energy upshift is attributed to the intervalley biexciton optical Stark effect because it exhibits three characteristics: (i) it emerges only within the pump pulse duration, (ii) it has a square-root dependence on the pump fluence, and (iii) it obeys the biexcitonic valley selection rule for opposite circularly polarized light, consistent with our model. Our results show that the intervalley biexciton is not only a rare and interesting quasiparticle by itself, but it also plays an active role to channel a coherent and valley-controllable light-matter interaction.

Apart from slight quantitative difference, the two types of optical Stark effects exhibit beautiful contrast and symmetry with the valley indices (K, K′) and the direction of the energy shift (down and up shifts). The optical Stark effect at K valley arises from intravalley exciton−exciton interaction through statistical Pauli repulsion, whereas the effect at K′ valley arises from intervalley exciton−exciton interaction through biexcitonic Coulomb attraction. Altogether, the two effects induce opposite energy shift at the two valleys, which is in contrast to the prior red-detuned optical Stark effect that occurs at only one valley.[5,6] This behavior is analogous to the Zeeman effect, which splits antisymmetrically the electronic valleys under

DOI: 10.1021/acs.nanolett.6b02998
Nano Lett. 2016, 16, 7421−7426

applied magnetic field.[36−39] We may therefore call this new phenomenon a Zeeman-type optical Stark effect in which the circularly polarized light plays the role of the magnetic field that breaks time-reversal symmetry and lifts the valley degeneracy (TOC graphic, also see Supporting Information). This new finding offers much insight into coherent light-matter interactions in TMD materials and may find important applications in the design of TMD-based photonic and valleytronic devices.

■ ASSOCIATED CONTENT

Supporting Information

The Supporting Information is available free of charge on the ACS Publications website at DOI: 10.1021/acs.nanolett.6b02998.

Transient absorption spectroscopy setup; optical contributions from the coherent and incoherent effects; time-trace fitting decomposition analysis; four-level Jaynes-Cummings model for the optical Stark effect; possible intervalley biexcitonic optical Stark effect under red-detuned pumping; fitting analysis based on the Jaynes-Cummings model; Zeeman-type optical Stark effect (PDF)

■ AUTHOR INFORMATION

Corresponding Author

*E-mail: gedik@mit.edu.

ORCID

Nuh Gedik: 0000-0002-6394-4987

Notes

The authors declare no competing financial interest.

■ ACKNOWLEDGMENTS

The authors acknowledge technical assistance by Qiong Ma and Yaqing Bie during the absorption measurement. N.G. and E.J.S. acknowledge support from the U.S. Department of Energy, BES DMSE (experimental setup and data acquisition) and from the Gordon and Betty Moore Foundation's EPiQS Initiative through Grant GBMF4540 (data analysis and manuscript writing). J.K. acknowledges support from STC Center for Integrated Quantum Materials, NSF Grant DMR-1231319 (material growth). Y.-H.L. thanks the funding support from AOARD grant (co-funded with ONRG) FA2386-16-1-4009, Ministry of Science and Technology (MoST 105-2112-M-007-032-MY3; MoST 105-2119-M-007-027), and Academia Sinica Research Program on Nanoscience and Nanotechnology, Taiwan (material growth).

■ REFERENCES

(1) Xiao, D.; Liu, G. B.; Feng, W.; Xu, X.; Yao, W. *Phys. Rev. Lett.* **2012**, *108*, 196802.

(2) Mak, K. F.; He, K.; Shan, J.; Heinz, T. F. *Nat. Nanotechnol.* **2012**, *7*, 494−498.

(3) Zeng, H.; Dai, J.; Yao, W.; Xiao, D.; Cui, X. *Nat. Nanotechnol.* **2012**, *7*, 490−493.

(4) Cao, T.; Wang, G.; Han, W.; Ye, H.; Zhu, C.; Shi, J.; Niu, Q.; Tan, P.; Wang, E.; Liu, B.; Feng, J. *Nat. Commun.* **2012**, *3*, 887.

(5) Sie, E. J.; McIver, J. W.; Lee, Y.-H.; Fu, L.; Kong, J.; Gedik, N. *Nat. Mater.* **2014**, *14*, 290−294.

(6) Kim, J.; Hong, X.; Jin, C.; Shi, S.-F.; Chang, C.-Y. S.; Chiu, M.-H.; Li, L.-J.; Wang, F. *Science* **2014**, *346*, 1205−1208.

(7) Mysyrowicz, A.; Hulin, D.; Antonetti, A.; Migus, A.; Masselink, W. T.; Morkoc, H. *Phys. Rev. Lett.* **1986**, *56*, 2748−2751.

(8) Von Lehmen, A.; Chemla, D. S.; Zucker, J. E.; Heritage, J. P. *Opt. Lett.* **1986**, *11*, 609−611.

(9) Mai, C.; Barrette, A.; Yu, Y.; Semenov, Y. G.; Kim, K. W.; Cao, L.; Gundogdu, K. *Nano Lett.* **2014**, *14*, 202−206.

(10) Sie, E. J.; Frenzel, A. J.; Lee, Y.-H.; Kong, J.; Gedik, N. *Phys. Rev. B: Condens. Matter Mater. Phys.* **2015**, *92*, 125417.

(11) Combescot, M.; Combescot, R. *Phys. Rev. Lett.* **1988**, *61*, 117−120.

(12) Hulin, D.; Joffre, M. *Phys. Rev. Lett.* **1990**, *65*, 3425−3428.

(13) Lee, Y.-H.; Zhang, X.-Q.; Zhang, W.; Chang, M.-T.; Lin, C.-T.; Chang, K.-D.; Yu, Y.-C.; Wang, J. T.-W.; Chang, C.-S.; Li, L.-J.; Lin, T.-W. *Adv. Mater.* **2012**, *24*, 2320−2325.

(14) Lee, Y.-H.; Yu, L.; Wang, H.; Fang, W.; Ling, X.; Shi, Y.; Lin, C.-T.; Huang, J.-K.; Chang, M.-T.; Chang, C.-S.; Dresselhaus, M.; Palacios, T.; Li, L.-J.; Kong, J. *Nano Lett.* **2013**, *13*, 1852−1857.

(15) Gutierrez, H. R.; Perea-López, N.; Elías, A. L.; Berkdemir, A.; Wang, B.; Lv, R.; López-Urías, F.; Crespi, V. H.; Terrones, H.; Terrones, M. *Nano Lett.* **2013**, *13*, 3447−3454.

(16) Li, Y.; Chernikov, A.; Zhang, X.; Rigosi, A.; Hill, H. M.; van der Zande, A. M.; Chenet, D. A.; Shih, E.-M.; Hone, J.; Heinz, T. F. *Phys. Rev. B: Condens. Matter Mater. Phys.* **2014**, *90*, 205422.

(17) Mai, C.; Semenov, Y. G.; Barrette, A.; Yu, Y.; Jin, Z.; Cao, L.; Kim, K. W.; Gundogdu, K. *Phys. Rev. B: Condens. Matter Mater. Phys.* **2014**, *90*, 041414.

(18) Wang, H.; Zhang, C.; Rana, F. *Nano Lett.* **2015**, *15*, 339−345.

(19) Schaibley, J. R.; Karin, T.; Yu, H.; Ross, J. S.; Rivera, P.; Jones, A. M.; Scott, M. E.; Yan, J.; Mandrus, D. G.; Yao, W.; Fu, K.-M.; Xu, X. *Phys. Rev. Lett.* **2015**, *114*, 137402.

(20) Wang, Q.; Ge, S.; Li, X.; Qiu, J.; Ji, Y.; Feng, J.; Sun, D. *ACS Nano* **2013**, *7*, 11087−11093.

(21) Sim, S.; Park, J.; Song, J.-G.; In, C.; Lee, Y.-S.; Kim, H.; Choi, H. *Phys. Rev. B: Condens. Matter Mater. Phys.* **2013**, *88*, 075434.

(22) Shi, H.; Yan, R.; Bertolazzi, S.; Brivio, J.; Gao, B.; Kis, A.; Jena, D.; Xing, H. G.; Huang, L. *ACS Nano* **2013**, *7*, 1072−1080.

(23) Pogna, E. A. A.; Marsili, M.; De Fazio, D.; Dal Conte, S.; Manzoni, C.; Sangalli, D.; Yoon, D.; Lombardo, A.; Ferrari, A. C.; Marini, A.; Cerullo, G.; Prezzi, D. *ACS Nano* **2016**, *10*, 1182−1188.

(24) Steinhoff, A.; Rösner, M.; Jahnke, F.; Wehling, T. O.; Gies, C. *Nano Lett.* **2014**, *14*, 3743−3748.

(25) The shifted absorption spectrum has the form of $\alpha(\omega, \Delta E) = \alpha(\omega - \Delta E)$. Hence, the absorption change before and after the shift is given by $\Delta\alpha(\omega, \Delta E) = \alpha(\omega - \Delta E) - \alpha(\omega) = -((\alpha(\omega) - \alpha(\omega - \Delta E))/\Delta E)\Delta E$, which can be written as $\Delta\alpha(\omega, \Delta E) = -(\mathrm{d}\alpha/\mathrm{d}\omega)\Delta E$.

(26) Stark, J. B.; Knox, W. H.; Chemla, D. S. *Phys. Rev. B: Condens. Matter Mater. Phys.* **1992**, *46*, 7919−7922.

(27) Crooker, S. A.; Awschalom, D. D.; Baumberg, J. J.; Flack, F.; Samarth, N. *Phys. Rev. B: Condens. Matter Mater. Phys.* **1997**, *56*, 7574−7588.

(28) Shang, J.; Shen, X.; Cong, C.; Peimyoo, N.; Cao, B.; Eginligil, M.; Yu, T. *ACS Nano* **2015**, *9*, 647−655.

(29) You, Y.; Zhang, X.-X.; Berkelbach, T. C.; Hybertsen, M. S.; Reichman, D. R.; Heinz, T. F. *Nat. Phys.* **2015**, *11*, 477−481.

(30) Kylänpää, I.; Komsa, H.-P. *Phys. Rev. B: Condens. Matter Mater. Phys.* **2015**, *92*, 205418.

(31) Xu, X.; Yao, W.; Xiao, D.; Heinz, T. F. *Nat. Phys.* **2014**, *10*, 343−350.

(32) Jaynes, E. T.; Cummings, F. W. *Proc. IEEE* **1963**, *51*, 89−109.

(33) Köster, N. S.; Kolata, K.; Woscholski, R.; Lange, C.; Isella, G.; Chrastina, D.; von Känel, H.; Chatterjee, S. *Appl. Phys. Lett.* **2011**, *98*, 161103.

(34) del Valle, E.; Zippilli, S.; Laussy, F. P.; Gonzalez-Tudela, A.; Morigi, G.; Tejedor, C. *Phys. Rev. B: Condens. Matter Mater. Phys.* **2010**, *81*, 035302.

(35) Schumacher, S.; Förstner, J.; Zrenner, A.; Florian, M.; Gies, C.; Gartner, P.; Jahnke, F. *Opt. Express* **2012**, *20*, 5335−5342.

(36) Li, Y.; Ludwig, J.; Low, T.; Chernikov, A.; Cui, X.; Arefe, G.; Kim, Y. D.; van der Zande, A. M.; Rigosi, A.; Hill, H. M.; Kim, S. H.; Hone, J.; Li, Z.; Smirnov, D.; Heinz, T. F. *Phys. Rev. Lett.* **2014**, *113*, 266804.

DOI: 10.1021/acs.nanolett.6b02998
Nano Lett. 2016, 16, 7421−7426

(37) MacNeill, D.; Heikes, C.; Mak, K. F.; Anderson, Z.; Kormányos, A.; Zólyomi, V.; Park, J.; Ralph, D. C. *Phys. Rev. Lett.* **2015**, *114*, 037401.
(38) Aivazian, G.; Gong, Z.; Jones, A. M.; Chu, R.-L.; Yan, J.; Mandrus, D. G.; Zhang, C.; Cobden, D.; Yao, W.; Xu, X. *Nat. Phys.* **2015**, *11*, 148−152.
(39) Srivastava, A.; Sidler, M.; Allain, A. V.; Lembke, D. S.; Kis, A.; Imamoğlu, A. *Nat. Phys.* **2015**, *11*, 141−147.

DOI: 10.1021/acs.nanolett.6b02998
Nano Lett. 2016, 16, 7421−7426